Supplement of Hydrol. Earth Syst. Sci., 21, 4115–4130, 2017
https://doi.org/10.5194/hess-21-4115-2017-supplement

Hydrology and Earth System Sciences
Open Access

Supplement of

Simulated hydrologic response to projected changes in precipitation and temperature in the Congo River basin

Noel Aloysius and James Saiers

Correspondence to: Noel Aloysius (aloysius.1@osu.edu)

1. Congo River Basin Hydrology Model

We use the Soil Water Assessment Tool [*Arnold et al.*, 1998], a physically-based, semi-distributed, watershed-scale model that operates at a daily time step, to simulate the hydrological processes in the Congo River Basin (CRB). The spatial heterogeneities are incorporated by dividing the river basin into smaller watersheds (n=1,575) and further dividing these watersheds into hydrologic response units (HRUs, n~8,500) based on land cover (16 classes) [*Bartholomé and Belward*, 2005], soils (150 types) [*FAO/IIASA*, 2009] and topography (90m digital elevation model) [*Lehner et al.*, 2008]. Gridded, one degree latitude /longitude horizontal resolution, daily values of minimum and maximum temperature and precipitation for the period 1948-2008 are used as climate inputs [*Sheffield et al.*, 2006]. The water balance in each HRU is calculated separately and aggregated at watershed level. Each watershed consists of one stream section to which the generated runoff (surface, lateral and groundwater) is routed. The runoff accumulated in each stream section is routed through the stream network using the variable storage routing method [*Neitsch et al.*, 2011]. We also include the wetlands and lakes (Figure 1 in the main text), which regulate the river flows at various locations, as unregulated storage reservoirs. A wetland is modeled as a storage structure that intercepts runoff only within the watershed where it is located, and is positioned off the stream section. Whereas, lakes (n=16, Table S1) receive water from all the upstream watersheds and are located on the stream [*Neitsch et al.*, 2011]. The potential evapotranspiration (PET) is estimated by Hargreaves method [*Hargreaves and Riley*, 1985]. The overland flow, percolation through the soil zone and lateral flow are modeled using the Soil Conservation Service curve number method (SCS-CN), a storage routing and a kinematic storage model, respectively [*Arnold et al.*, 1998; *Neitsch et al.*, 2011; *USDA Soil Conservation Service*, 1972]. In SCS-CN method, overland flow (q_s) is defined as

$q_s = \frac{(R-\lambda S)^2}{(R-(1-\lambda)S)}$ when $R > \lambda S$ and $q_s = 0$ otherwise, where R is the daily rainfall, S is the retention parameter which varies due to changes in soil type, land cover, slope and changes in soil water content and λ is the initial abstraction ratio. The value of S is transformed to the curve number (CN) by the formulation $S = 25.4\left(\frac{1000}{CN} - 10\right)$. Recent studies suggest that the value for λ should more appropriately be near 0, as opposed to current value of 0.2 [*Hawkins et al.*, 2009; *Lamont et al.*, 2008]. In this study we set $\lambda = 0.01$, and the curve numbers for different land cover types were estimated by calibration. The relationship between water-spread area of lakes and the corresponding storage volume is modeled as $A = aV^b$, where, A and V are area and volume, and a and b are parameters estimated by calibration. The relationship between outflows from the lakes and the storage volume is modeled as $q_l = a_1 V^{b_1}$, where, q_l is the outflow from lakes and a_1 and b_1 are parameters estimated by calibration. The nonlinear groundwater storage and discharge response at HRU level is modeled as q= $\sqrt[(2-b_2)]{\left((2-b_2)a_2(S-S_o)\right)}$, where q is the groundwater contribution to the total runoff generated within an HRU, S is the shallow aquifer storage and S_o is the minimum aquifer storage required for groundwater flow and a_2 and b_2 (< 2.0) are parameters (see similar approach in *Kirchner* [2009]). Values for S_o, a_2 and b_2 are estimated by calibration. All the revisions are implemented in version 488 of the model source code and compiled using Intel© FORTRAN compiler. Model parameters estimated by calibration are provided in Table S6.

Accessible streamflows (AF), at monthly time steps were estimated by applying baseflow filter technique described in *Nathan and McMahon* [1990].

2. Temporal Downscaling of Climate Variables

We use three-hourly and monthly observed climate fields [*Sheffield et al.*, 2006] and bias-corrected monthly climate fields to temporally downscale the bias-corrected three-hourly fields, following the method described in *Sheffield et al.* [2006]. The precipitation fields are scaled as follows:

$$P_{BC,3hr} = \frac{P_{BC,mon}}{P_{Obs,mon}} \times P_{Obs,3hr} \quad (1)$$

where P is precipitation, *3hr* and *mon* indicate three-hourly and monthly values, and *BC* and *Obs* indicate bias-corrected GCM simulations and observations, respectively. The three-hourly values are summed to obtain daily precipitation.

The temperature values are disaggregated to three-hourly values using a two-step procedure, in order to scale with the monthly mean temperature and the diurnal temperature range, as follows:

$$T_{BC,3hr} = T_{Obs,3hr} + \left(T_{BC,mon} - T_{Obs,mon}\right) \quad (2)$$

$$T_{BC,3hr} = T_{BC,daily} + \frac{DTR_{BC,mon}}{DTR_{Obs,mon}} \times \left(T_{BC,3hr} - T_{BC,daily}\right) \quad (3)$$

where T and DTR are temperature and diurnal temperature range, respectively. The daily average temperature used in (3) is computed from the three-hourly temperature in (2). The daily minimum and maximum temperatures are extracted from the three-hourly values computed in (3).

3. Supplementary Tables

Table S1 Area, volume and annual mean precipitation in lakes used in this study.

Lake Name (Latitude/Longitude)	Area (km^2)	Volume (km^3)	Average annual rainfall[1] (mm)	Key references
Bangweulu (11.8S, 29.9E)	3,900	8.2	1,300	*Burgis and Symoens [1987]*, *Lehner and Döll* [2004], *Serruya and Pollingher* [1983] and *Tilzer and Serruya* [1990]
Kabamba (7.8S, 26.9E)	170	2.6	1,360	*Lehner and Döll* [2004]
Kabele (8.8S, 26.2E)	100	5.7	1,600	*Lehner and Döll* [2004]
Kabwe (9.0S, 26.0E)	100	1.9	1,200	*Lehner and Döll* [2004]
Kisale (8.1S, 26.8E)	260	7.2	1,600	*Lehner and Döll* [2004]
Kivu (2.5S, 28.9E)	2,500	570	1,300	*Lehner and Döll* [2004], *Lempicka* [1971], *Serruya and Pollingher* [1983] and *Tilzer and Serruya* [1990]
Mai Ndombe (2.7S, 18.1E)	2,200	11.4	1,600	*Lehner and Döll* [2004], *Serruya and Pollingher* [1983] and *Tilzer and Serruya* [1990]
Mwadingusha (10.7S, 27.3E)	410	1	1,030	*Lehner and Döll* [2004], *Magis* [1961] and *Serruya and Pollingher* [1983]
Mweru (8.5S, 28.8E)	4,700	38	1,100	*Bos et al.* [2006], *Lehner and Döll* [2004], *Serruya and Pollingher* [1983] and *Tilzer and Serruya* [1990]

Mweru Wantipa (9.0S, 29.4E)	1,450	8	1,100	*Burgis and Symoens [1987]*, *Lehner and Döll* [2004], *Tilzer and Serruya* [1990]
Nzilo (10.4S, 25.4E)	230	2	1,100	*Crul* [1992], *Lehner and Döll* [2004], *Serruya and Pollingher* [1983] and *Magis* [1961]
Tanganyika (5.9S, 29.1E)	32,000	18,900	1,100	*Lempicka* [1971], *Lehner and Döll* [2004], *Serruya and Pollingher* [1983] and *Tilzer and Serruya* [1990]
Tele (1.1S, 17.0E)	23	0.071	1,600	[*Laraque et al.*, 1998] and *Lehner and Döll* [2004]
Tumba (0.6S, 17.8E)	610	3	1,540	*Burgis and Symoens [1987]*, *Lehner and Döll* [2004], *Serruya and Pollingher* [1983] and *Tilzer and Serruya* [1990]
Upemba (8.4S, 26.4E)	550	1.3	1,600	*Burgis and Symoens [1987]*, *Lehner and Döll* [2004], *Serruya and Pollingher* [1983] and *Tilzer and Serruya* [1990]
Zimbambo (8.0S, 27.0E)	200	4.8	1,600	*Lehner and Döll* [2004]

[1]annual average rainfall in the watershed where the lake is located

Table S2 Annual and season values of precipitation and runoff in the CRB and four regions identified in Figure 1 in the main text for the reference period 1986-2005. The values are based on the multi-model mean (n=25). All values in mm per year/season.

	Congo (CRB)	Northern (NC)	Equatorial (EQ)	Southwestern (SW)	Southeastern (SE)
Precipitation					
Annual	1,439	1,453	1,599	1,359	1,110
DJF	368	34	332	505	561
MAM	410	356	464	419	307
JJA	219	582	280	16	4
SON	442	481	523	418	239
Runoff					
Annual	382	241	515	410	125
DJF	103	31	134	133	49
MAM	103	17	130	151	53
JJA	71	68	103	55	10
SON	105	126	149	72	13

Table S3 Nash-Sutcliff model efficiency coefficients describing the predictive power of streamflows by the Congo River Basin hydrological model. Gage locations and the comparison of observed and simulated annual runoff within the catchment areas are presented in the main text as Figures 1 and 3.

Gage name	River name	Latitude	Longitude	Catchment area (km^2)	Nash-Sutcliffe model efficiency coefficient
Zemio	Mbomou	5.0300	25.1500	27,840	0.07
Rafai	Chinko	4.9700	23.9200	52,834	0.72
Bossele-Bali	M'Poko	4.5300	18.4700	10,670	0.30
Pana	Kadei	4.2000	14.6800	21,251	0.68
Batouri	Kadei	4.2300	14.3200	9,833	0.65
Bangui	Ubangi	3.3583	18.5958	52,1344	0.86
Somalomo	Dja	3.3800	12.7700	5,088	0.01

Salo	Sangha	3.1800	16.1000	71,152	0.48
Ngbala	Dja	2.0200	14.9000	39,330	0.07
Ouesso	Sangha	1.6200	16.0500	158,170	0.64
Kisangani	Congo	0.5056	25.1917	979,731	0.04
Ponthierville	Congo (ex-Lualaba)	-0.3819	25.4750	941,079	0.57
Opala	Lomami	-0.6028	24.3528	91,396	0.51
Lowa	Congo (ex-Lualaba)	-1.4000	25.8639	923,045	0.58
Bukavu-Ruzizi	Ruzizi	-2.4903	28.8922	7,673	0.09
Lediba	Kasai	-3.0569	16.5569	888,601	0.60
Kutu-Moke	Kasai	-3.1972	17.3458	744,952	0.77
Gatumba	Rusizi	-3.3333	29.2500	12,467	0.22
Kindu	Congo (ex-Lualaba)	-2.9528	25.9292	798,468	0.29
Bandundu	Kwango	-3.2986	17.3708	270,052	0.37
Kinshasa	Congo	-4.3000	15.3000	3,614,731	0.34
Port Franqui	Kasai	-4.3333	20.5819	245,170	0.69
Kasongo	Congo (ex-Lualaba)	-4.5306	26.5778	758,473	0.54
Inkisi Pont-route	Inkisi	-5.1292	15.0681	12,743	0.30
Boma	Congo	-5.8583	13.0500	3,679,979	0.43
Kiambi	Luvua	-7.3375	28.0125	244,581	0.75
Mulongo	Congo (ex-Lualaba)	-7.8417	26.9764	160,764	0.53
Bukama	Congo (ex-Lualaba)	-9.1931	25.8597	62,922	0.42
Kasenga	Luapula	-10.3597	28.6153	160,200	0.76
Chembe Ferry	Luapula	-11.9666	28.7500	122,703	0.47

Table S4 Multi-model mean (MM) changes in projected runoff (%) in selected regions (within the four regions identified in Figure 1) for the near-term (2016-2035) and the mid-term (2046-2065) relative to the reference period of 1986-2005. The approximate locations are identified by latitudes and longitudes. Number of GCMs used in the multi-model mean is 25. The standard deviation is provided in parenthesis. DJF: Dec-Jan-Feb, MAM: Mar-Apr-May, JJA: Jun-Jul-Aug and SON: Sep-Oct-Nov. We calculated the area-averaged mean for each GCM ensemble before computing the multi-model mean.

	RCP45			RCP85		
	Northeast	Equatorial west	Southern sub region	Northeast	Equatorial west	Southern sub region
	(3.5N-9N and 25E-33E)	(1.5S-2.5N and 17E-21E)	(10S-14S and 26E-33E)	(3.5N-9N and 25E-33E)	(1.5S-2.5N and 17E-21E)	(10S-14S and 26E-33E)
Near-term (2016-2035)						
Annual	-1.2 (11.8)	0.23 (7.1)	-10.27 (28)	-5.23 (14.7)	-0.27 (6.4)	-10.13 (27.2)
DJF	11.72 (15.9)	0.2 (10.9)	-6.59 (19.8)	10.1 (20)	-0.49 (9.5)	-6.63 (20.6)
MAM	7.52 (14.4)	1.7 (7.8)	-12.27 (33)	2.19 (16.8)	1.51 (4.6)	-11.28 (31.5)
JJA	-8.54 (12.8)	-1.26 (7.9)	-12.78 (35.1)	-12.88 (14.6)	-0.09 (7.6)	-12.8 (31.9)
SON	-0.76 (12.9)	0.58 (8.8)	-7.1 (24.3)	-4.86 (16.4)	-1.11 (10)	-12.98 (18.5)
Mid-Term (2046-2065)						
Annual	-1.9 (19)	-2.03 (7.9)	-13.84 (35.2)	-5.93 (23.1)	-0.82 (9.4)	-14.4 (39.7)
DJF	8.32 (23.5)	-0.34 (11.5)	-11.04 (24.8)	3.26 (27.9)	4.29 (15.1)	-10.61 (30.7)
MAM	19.57 (25.2)	0.84 (7.5)	-14.96 (41.2)	19.63 (25.5)	0.96 (6.9)	-15.51 (45.6)
JJA	-6.14 (21.2)	-1.5 (10.9)	-16.76 (43.6)	-9.08 (23.7)	-0.94 (13)	-18.76 (47.8)
SON	-4.27 (19.6)	-4.91 (8.8)	-14.48 (26.3)	-9.52 (24.2)	-4.68 (10.4)	-16.82 (25.4)

Table S5 Select-model mean (SM) changes in projected runoff (%) in selected regions (within the four regions identified in Figure 1) for the near-term (2016-2035) and the mid-term (2046-2065) relative to the reference period of 1986-2005. The approximate locations are identified by latitudes and longitudes. Number of GCMs used in the multi-model mean is 25. The standard deviation is provided in parenthesis. DJF: Dec-Jan-Feb, MAM: Mar-Apr-May, JJA: Jun-Jul-Aug and SON: Sep-Oct-Nov. We calculated the area-averaged mean for each GCM ensemble before computing the multi-model mean.

	RCP45			RCP85		
	Northeast (3.5N-9N and 25E-33E)	Equatorial west (1.5S-2.5N and 17E-21E)	Southern sub region (10S-14S and 26E-33E)	Northeast (3.5N-9N and 25E-33E)	Equatorial west (1.5S-2.5N and 17E-21E)	Southern sub region (10S-14S and 26E-33E)
Near-term (2016-2035)						
Annual	5.94 (13.5)	6.42 (9.4)	-9.43 (18.7)	1.05 (12.5)	4.77 (10.3)	-1.2 (17.3)
DJF	16.75 (15)	12.02 (16.1)	-9.03 (15.4)	20.54 (15.1)	9.04 (15.8)	-1.08 (14)
MAM	8.76 (9.1)	2.66 (5.2)	-10.13 (20.9)	0.91 (7.8)	-1.47 (5.1)	-0.47 (20.5)
JJA	-1.52 (17.1)	3.18 (7.4)	-7.04 (19.6)	-11.09 (12)	3.37 (7.6)	-1.23 (15.4)
SON	7.86 (13.8)	8.1 (13)	-10.65 (18.7)	4.08 (14)	7.74 (16.8)	-10.77 (13.9)
Mid-Term (2046-2065)						
Annual	2.86 (11.1)	3.63 (7.5)	-8.94 (24.4)	8.02 (22.6)	6.43 (8.8)	-7.63 (25.2)
DJF	13.74 (15.9)	10.66 (11.4)	-7.87 (19.2)	18.68 (18.6)	17.02 (11.9)	-4.93 (14.8)
MAM	18.88 (9.6)	0.11 (9.3)	-8.68 (28.2)	27.57 (16.3)	1.76 (7.3)	-8.13 (30.8)
JJA	-3.47 (15.2)	1.16 (6.3)	-8.62 (24.3)	2.19 (29.6)	7.37 (11.2)	-8.88 (29.6)
SON	2.24 (10.8)	3.8 (10.5)	-21.26 (19.3)	6.72 (22.9)	2.88 (10.9)	-19.32 (14.2)

Table S6 List of parameters included in the model calibration and their ranges.

Parameter	Input file	Spatial Level	Description	Range / Default value	Calibrated values
λ		HRU	This parameter affects the amount of surface runoff generated at HRU-level. Initial abstractions include surface storage, interception and infiltration prior to runoff. The value is commonly approximated as 0.2.	0.2	0.01*
CN2	.mgt	HRU	Initial Soil Conservation Service moisture condition II curve number. This value varies between 30 and 98 for λ=0.2 and are appropriate for 5% slope.	30-98	10-80
EPCO	.hru	Watershed	Plant uptake compensation factor. High values allow water uptake from soil layers to meet the plant demand.	0.01-1.0	0.12-1.0
ESCO	.hru	HRU	Soil evaporation compensation factor. At low values, the model is able to draw more water from soil layers.	0.01-1	0.11-0.90
HRU_SLP	.hru	HRU	Average slope steepness (m/m)	0-1	Slope derived based on the topography (DEM) is adjusted by a percentage at HRU level. -19% to 30%
OVN	.hru	HRU	Manning's "n" value for overland flow	0.008-0.5	0.01-0.2
GW_DELAY	.gw	HRU	Delay time for aquifer recharge (days). This parameter gives the lag time when water exits the soil profile and enters the shallow aquifer.	0-50	23-50
GW_REVAP	.gw	HRU	Revap coefficient. This parameter controls the amount of water that moves from shallow aquifer to the root zone. At high values allow for more water available to plants.	0.02-2	0.02-0.2
REVAPMN	.gw	HRU	Threshold water level in shallow aquifer above which water is available for plant evapotranspiration (mm H_2O)	0-500	1-40
b2	.gw	HRU	Constant for groundwater contribution to stream flow	0-1.99	0.4-1.99
GWQMN	.gw	HRU	Threshold depth of shallow aquifer storage for baseflow to occur (mm H2O)	0-5000	1-50
RCHRG_DP	.gw	HRU	Fraction of percolation from the root zone that recharges the deep aquifer	0-1	0.002-0.17
a2	.gw	HRU	Constant for groundwater contribution to stream flow	.01-10	0.01-1.5
SOL_AWC	.sol	HRU	Available water capacity of soil layer	0-1	-50% - 50%, value is adjusted by a percentage at HRU level.

SOL_K	.sol	HRU	Saturated hydraulic conductivity (mm/hr)	0.75-1.25	-15% - 50%, value is adjusted by a percentage at HRU level
EVP	.res	Reservoir	Lake evaporation coefficient. Evaporation depth is estimated by multiplying this coefficient by the potential evapotranspiration	0-1	0.3-0.9
WK	.pnd	Wetland	Hydraulic conductivity of wetland bottom surface (mm/hr)	0-1	0.01-0.7
WEVP	.pnd	Wetland	Wetland evaporation coefficient	0-1	0.41-0.7

* fixed throughout the simulation

4. Supplementary Figures

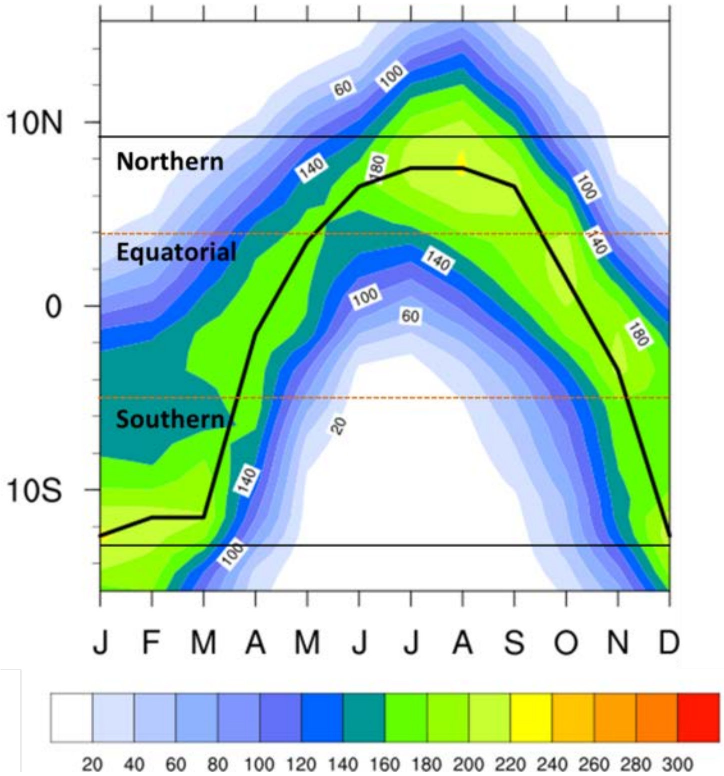

Figure S1 Zonally (11.5^{o}E – 34.5^{o}E) averaged monthly precipitation over Central Africa. Monthly values are 1971-2000 averages obtained from *Sheffield et al.* [2006]. The black horizontal lines show the latitudinal boundaries of the Congo River Basin. The red dotted lines separate the Northern, Equatorial and Southern regions identified in Figure 1 in the main text.

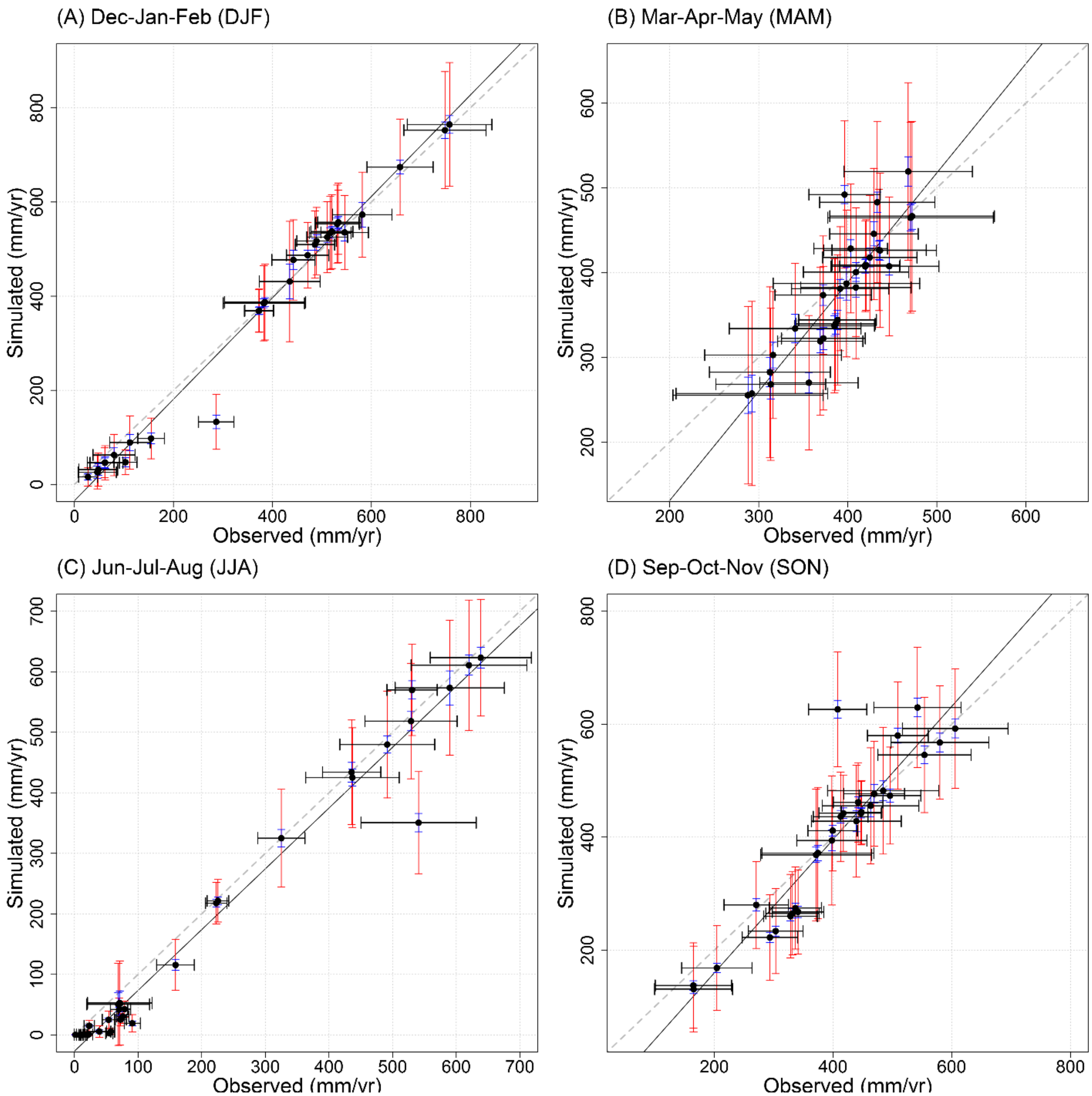

Figure S2 Observed and GCM-simulated seasonal precipitation averaged over the catchment areas of 30 stream flow gages in Figure 1 in the main text: (A) Dec-Jan-Feb, (B) Mar-Apr-May, (C) Jun-Jul-Aug and (D) Sep-Oct-Nov). Black dots compare multi-model means with observed precipitation, black horizontal bars show observed inter-annual variability, and red (blue) vertical bars show maximum (minimum) range of modeled inter-annual variability among the 25 climate model outputs. The GCM-simulated forcings are statistically downscaled and bias-corrected.

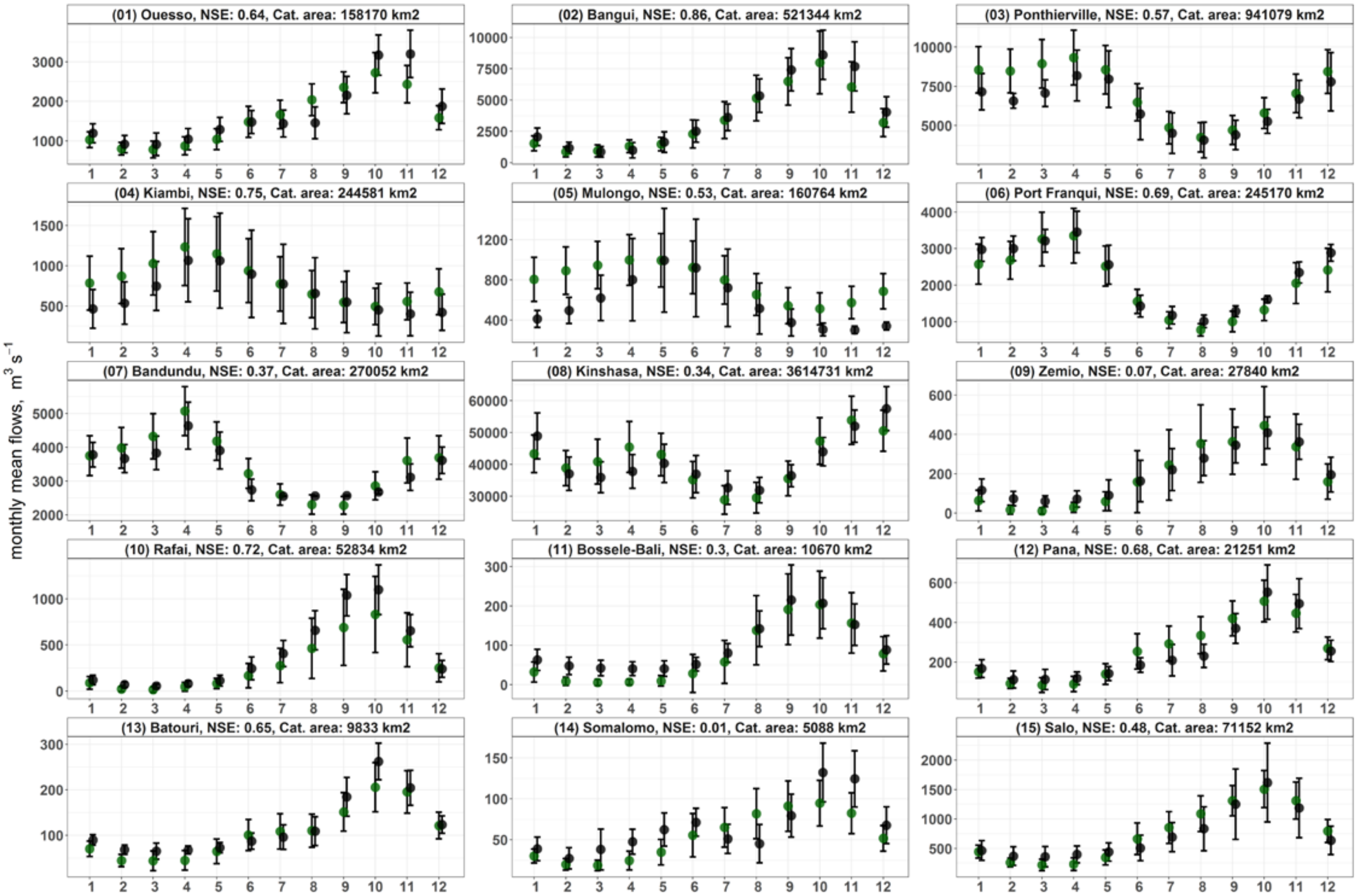

Figure S3 Monthly stream flow hydrographs at 30 flow gage locations in Figure 1 for the period 1950-2008, the black (green) filled circles are observed (simulated) flows. NSE – Nash-Sutcliff model efficiency values, a measure of relative magnitude of residual variance compared to the observed flow variance, and catchment areas above each gage are also given. Monthly mean flows are in m^3/s. Plot numbers 1-8 coincide with the gages identified in Figure 1 in the main text.

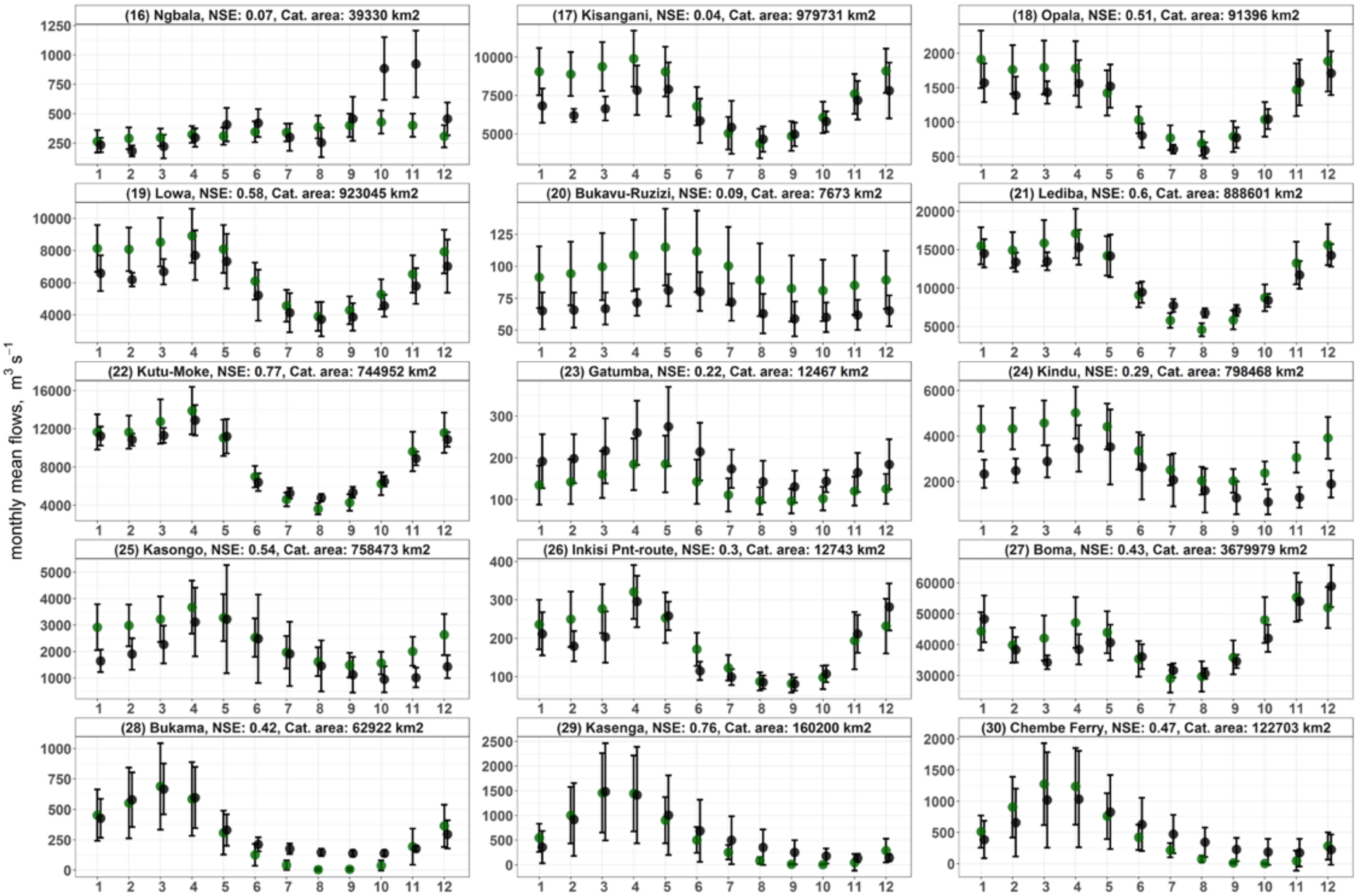

Figure S3 continued.

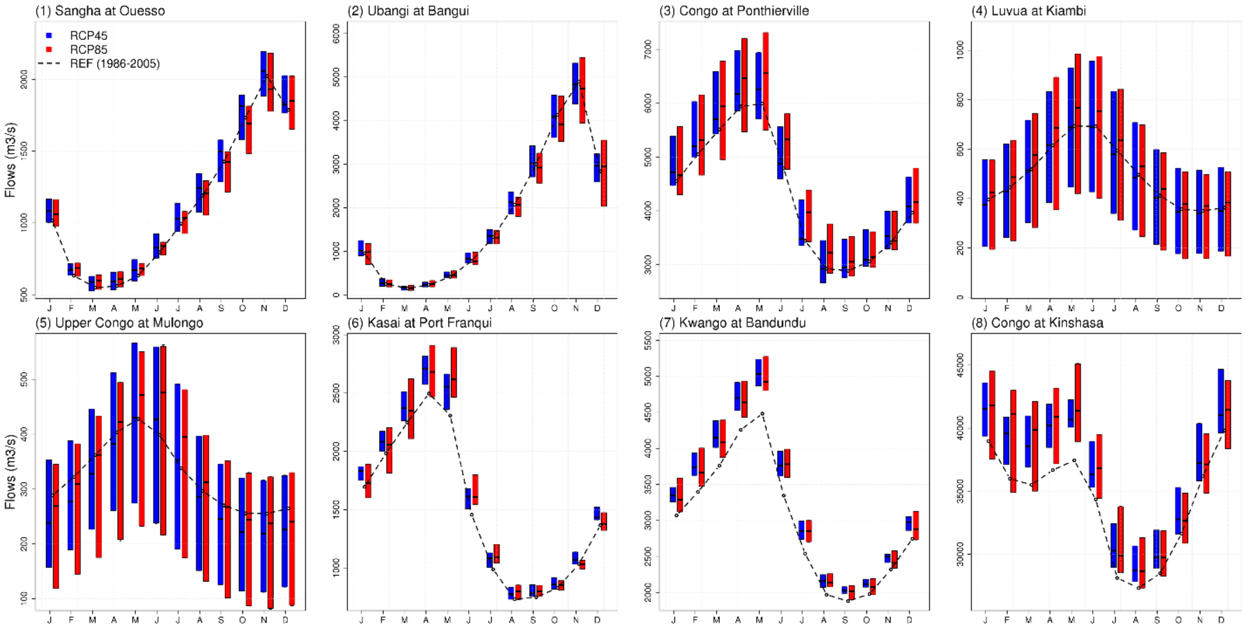

Figure S4 Accessible stream flow hydrographs in the mid-term at selected locations shown in Figure 1. Blue (red) bars show the inter-model variability. Dotted black line shows the hydrograph in the reference period (1986-2005). Figure numbers 1-8 coincide with the gage numbers in Figure 1.

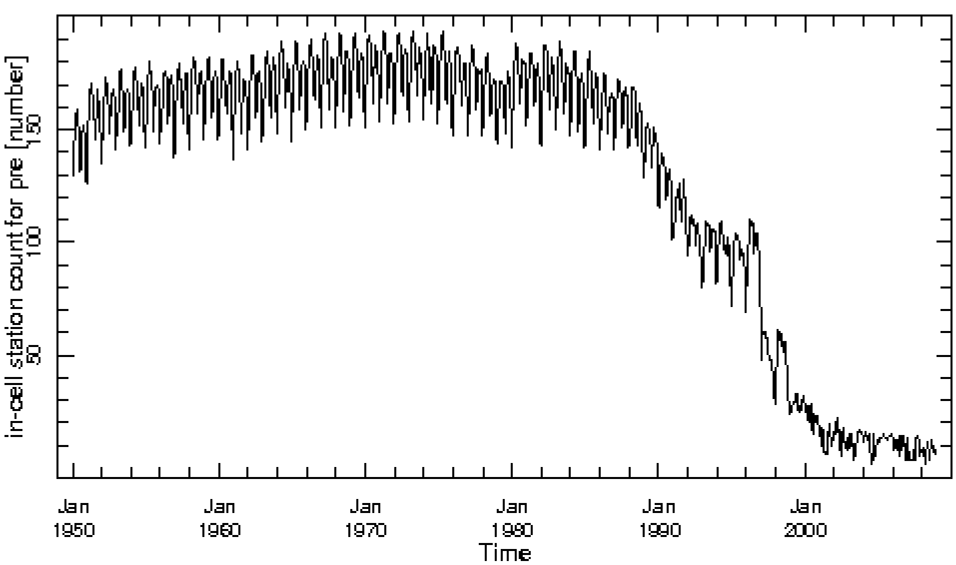

Figure S5 Total number of precipitation gages used to develop the observed climate data. Y-axis shows the number of gage stations lie within the 0.5x0.5 latitude/longitude grids with the study area (9N-14S and 12E-

32E). These monthly totals, as reported in *Harris et al.* [2013] and *Sheffield et al.* [2006], are obtained from the IRI Data Library [*Lamont-Doherty Earth Observatory Climate Group*, 2017]. Accessed on Jan 31, 2017.

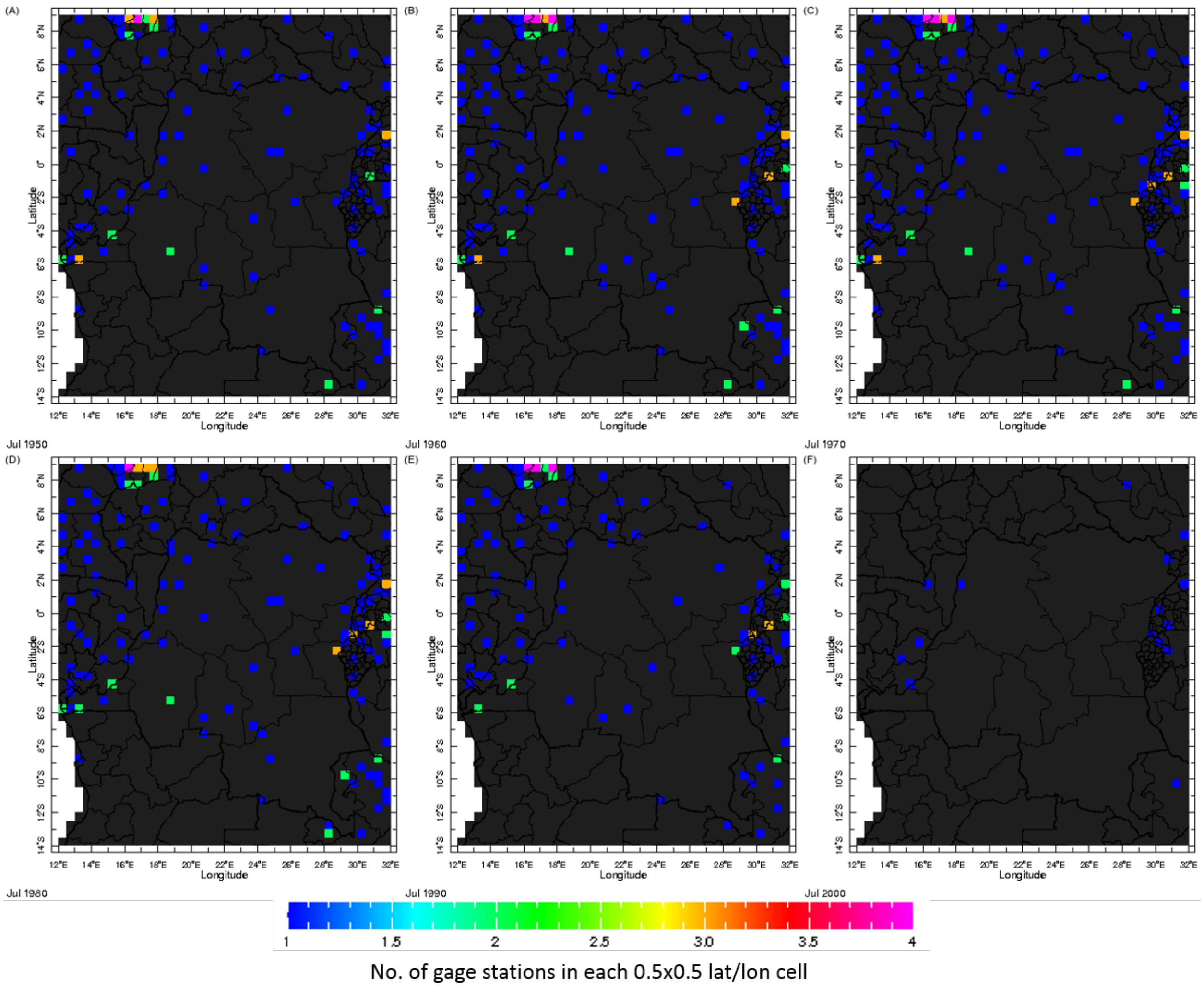

Figure S6 Distribution of precipitation gages in Central Africa from 1950 to 2000. Each color pixel shows the number of gage stations lie within the 0.5x0.5 latitude/longitude grids. No data are shown in grey. These observations, as reported in *Harris et al.* [2013], are obtained from the IRI Data Library [*Lamont-Doherty Earth Observatory Climate Group*, 2017]. Accessed on Jan 31, 2017.

5. References

Arnold, J. G., R. Srinivasan, R. S. Muttiah, and J. R. Williams (1998), Large area hydrologic modeling and assessment part I: Model development, *Journal of the American Water Resources Association*, *34*(1), 73-89.

Bartholomé, E., and A. S. Belward (2005), GLC2000: A new approach to global land cover mapping from Earth observation data, *International Journal of Remote Sensing*, *26*(9), 1959-1977.

Bos, A. R., C. K. Kapasa, and P. A. M. Van Zwieten (2006), Update on the bathymetry of Lake Mweru (Zambia), with notes on water level fluctuations, *African Journal of Aquatic Science*, *31*(1), 145-150.

Burgis, M. J., and J. J. Symoens (Eds.) (1987), *African Wetlands and Shallow Water Bodies*, 650 pp., Institut Francais de Recherche Scientifique pour le Development en Cooperation, Paris.

Crul, R. C. M. (1992), Models for estimating potential fish yields of African inland waters*Rep. CIFA Occational Paper No. 16*, Food and Agricultural Organization of the United Nations, Rome, Italy.

FAO/IIASA (2009), Harmonized World Soil Database (version 1.1), in *Food and Agricultural Organization and IIASA*, edited, Rome, Italy and Laxenburg, Austria.

Hargreaves, G., and J. Riley (1985), Agricultural Benefits for Senegal River Basin, *Journal of Irrigation and Drainage Engineering*, *111*(2), 113-124.

Harris, I., P. D. Jones, T. J. Osborn, and D. H. Lister (2013), Updated high-resolution grids of monthly climatic observations – the CRU TS3.10 Dataset, *International Journal of Climatology*, *34*(3), 623-642.

Hawkins, R., T. Ward, D. Woodward, and J. Van Mullem (2009), *Curve Number Hydrology*, American Society of Civil Engineers, Reston, VA.

Kirchner, J. W. (2009), Catchments as simple dynamical systems: Catchment characterization, rainfall-runoff modeling, and doing hydrology backward, *Water Resour. Res.*, *45*.

Lamont-Doherty Earth Observatory Climate Group (2017), *IRI/LDEO climate data library - http://iridl.ldeo.columbia.edu/*, Lamont-Doherty Earth Observatory (LDEO) Climate Group, Columbia University, Palisades, NY.

Lamont, S. J., R. N. Eli, and J. J. Fletcher (2008), Continuous hydrologic models and curve numbers: A path forward, *Journal of Hydrologic Engineering*, *13*(7), 621-635.

Laraque, A., et al. (1998), Origin and function of a closed depression in equatorial humid zones: The Lake Tele in North Congo, *Journal of Hydrology*, *207*(3-4), 236-253.

Lehner, and P. Döll (2004), Development and validation of a global database of lakes, reservoirs and wetlands, *Journal of Hydrology*, *296*(1–4), 1-22.

Lehner, K. Verdin, and A. Jarvis (2008), New Global Hydrography Derived from Spaceborne Elevation Data, *Eos. Trans. AGU*, *89*(10).

Lempicka, M. (1971), Bilan hydrique du bassin du fleuve Zaire. *Rep.*, Office National de la Recherche et du Development, Kinshasa, DRC.

Magis, N. (1961), Nouvelle contribution à l'étude hydrobiologique des lacs de Mwadingusha, Koni et N'Zilo. *Rep.*, Université de Liège. Fondation de l'Université de Liège pour les recherches scientifiques en Afrique Centrale (FULREAC).

Nathan, R. J., and T. A. McMahon (1990), Evaluation of automated techniques for base flow and recession analyses, *Water Resources Research*, *26*(7), 1465-1473.

Neitsch, S. L., J. G. Arnold, J. R. Kiniry, and J. R. Williams (2011), Soil Water Assessment Tool - Theoretical Documentation - Version 2009*Rep. 406*, 647 pp, Texas Water Resources Institute, Texas A&M University, Temple, Texas.

Serruya, C., and U. Pollingher (1983), Africa, in *Lakes of the Warm Belt*, edited, pp. 131-284, Cambridge University Press, Cambridge, UK.

Sheffield, J., G. Goteti, and E. F. Wood (2006), Development of a 50-year high-resolution global dataset of meteorological forcings for land surface modeling, *Journal of Climate*, *19*(13), 3088-3111.

Tilzer, M. M., and C. Serruya (1990), *Large Lakes: Ecological Structure and Function*, 691 pp., Springer-Verlag, Berlin.

USDA Soil Conservation Service (1972), Section 4: Hydrology, in *National Engineering Handbook*, edited, United States Department of Agriculture (USDA), Washington, D.C.